Imaging of Microscopic Sources of Resistive and Reactive Nonlinearities in Superconducting Microwave Devices

Alexander P. Zhuravel, Steven M. Anlage, *Member, IEEE*, and Alexey V. Ustinov

Abstract—**The technique of low-temperature Laser Scanning Microscopy (LSM) has been applied to the investigation of local microwave properties in operating $\mathrm{YBa_2Cu_3O_7/LaAlO_3}$ thin-film resonators patterned into a meandering strip transmission line. By using a modified newly developed procedure of spatially-resolved complex impedance partition, the influence of inhomogeneous current flow on the formation of nonlinear (NL) microwave response in such planar devices is analysed in terms of the independent impact from resistive and inductive components. The modified procedure developed here is dramatically faster than our previous method. The LSM capability to probe the spatial variations of two-tone, third-order intermodulation photoresponse on micron length scales is used to find the 2D distribution of the local sources of microwave NL. The results show that the dominant sources of microwave NL are strongly localized in the resistive domains.**

Index Terms—**High-$\mathrm{T_c}$ superconductors, intermodulation, laser scanning microscopy, microwave devices, nonlinearity.**

I. INTRODUCTION

IDENTIFICATION of *microscopic* sources of resistive and reactive nonlinearities (NLs) in high-temperature superconducting (HTS) films, as well as clarification of the distinct role that such sources are playing in the *macroscopic* (integral) response of passive microwave devices, is a vital issue of fundamental and applied research for HTS materials in high-frequency (HF) fields. For example, the examination of the nonlinear Meissner effect (NLME) for evidence of d-wave gap symmetry in the cuprates [1] is facilitated by inductive NL at current-carrying strip edges. In turn, the HF current-dependent topology of the *microscopic* sources of resistive NLs is significant for explanation of NL response of a HTS device in the critical state [2]. And finally, improvement of microwave device technology comes from a thorough understanding of the

contribution of different defects, the topology of dc and rf transport, as well as geometrical and structural inhomogeneities.

We have shown earlier that the low-temperature Laser Scanning Microscope (LSM) is a powerful nondestructive evaluation technique for non-contact, spatially-resolved probing of the local HF current density, $J_{\mathrm{HF}}(x,y)$ in HTS films and devices [3]. This LSM method was applied next for mapping optical, thermal, HF and dc electron transport properties and superconducting critical parameters of HTS samples directly in their operating state at $T < T_c$, with micron-scale spatial resolution [4]. Furthermore, a procedure of spatially-resolved partition of its resistive and inductive photo-response (PR) components is developed in [5], while a procedure of LSM PR(x,y) calibration to determine the absolute amplitude of $J_{\mathrm{HF}}(x,y)$ is described in [4].

In this paper, we develop a new procedure of rapid, spatially-resolved LSM analysis of HTS devices in varied HF fields to investigate the 2D distribution of the local sources of microwave NL in a microstrip-line resonator. Our results show that a spatial topology of dominant NL sources is correlated with the microwave-field-dependent distribution of the resistive domains formed by regions of local overcritical current densities in the superconducting strip.

II. EXPERIMENTAL DETAILS

A. Sample

The sample is a $\mathrm{YBa_2Cu_3O_y}$ (YBCO) film with thickness of about 1 μm configured by ion-milling lithography on $\mathrm{LaAlO_3}$ (LAO) substrate into a meandering strip line resonator with line width of 250 μm. The geometry of the resonator is shown in Fig. 1. The frequency of fundamental resonance is about 1.85 GHz. Here, we give an example of LSM characterization of the resonator at the third harmonic frequency (the fundamental is outside the bandwidth constraints of the instrumentation) of about 5.96 GHz where it demonstrates a loaded $Q_L \sim 2000$ at T = 80 K. The device is capacitively coupled to an input RF circuit delivering power P_{IN} in the range from -40 to $+10$ dBm and mounted in a copper microwave package. The package was cooled inside the vacuum cavity of an optical cryostat which stabilizes the temperature of the sample in the range 77–95 K with an accuracy better then 5 mK [3], [4].

B. Imaging Procedures

The LSM studies were performed by $x-y$ scanning of the resonator surface by a 1.1 μm diameter laser beam. The power of
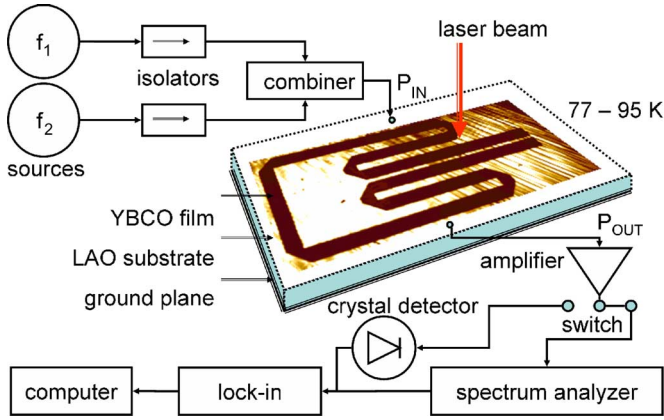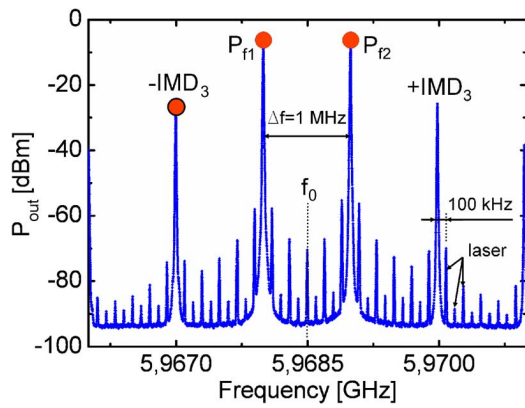
Fig. 1. Schematic of the microwave LSM experiment.

Fig. 2. Spectrum of output signal for $P_{IN}(f_1) = P_{IN}(f_2) = +12$ dBm, $T = 78$ K, and $f_1 = 5.968$ GHz, $f_2 = 5.969$ GHz, and $f_M = 100$ kHz.

the laser $P_L = 10\ \mu$W was fixed low enough to introduce minimal perturbation on the global microwave properties of the resonator. The intensity of the laser is modulated at a frequency of $f_M = 100$ kHz, producing an oscillating thermal probe of about $4\ \mu$m in diameter [3], [4], [6], [7]. Fig. 1 shows a schematic of the experiment. Two fixed frequency signals (f_1 and f_2) are applied to the HTS resonator. These signals are centered on the $|S_{21}(f)|$ curve with an equal spacing $\pm\Delta f/2 = 500$ kHz around the device resonant frequency f_0 and have the same amplitude $P_{IN}(f_1) = P_{IN}(f_2)$.

Transmitted HF signals are amplified and measured by a spectrum analyser, as shown in Fig. 2. In addition to P_{f1} and P_{f2} output tones, the spectrum of the resonator contains intermodulation harmonics $-IMD_3 = P_{2f1-f2}$ and $+IMD_3 = P_{2f2-f1}$ resulting from NL mixing of the signals at f_1 and f_2, as well as laser modulation sidebands. A zero-frequency span mode of the spectrum analyser combined with a lock-in amplifier technique was used to separate the probe-induced modulation of the output spectrum (so-called LSM photoresponse, PR) at different f specified by the filled circles in Fig. 2. Changes in P_{f1} and P_{f2} as a function of position (x, y) of the laser beam perturbation on the sample were collected to build up 2D maps of both resistive and inductive components of LSM PR in compliance with the partition method described in [5]. The intermodulation (IMD) imaging LSM mode was applied to image the distribution of *microscopic* sources of NL response at $\pm IMD_3$ [6].
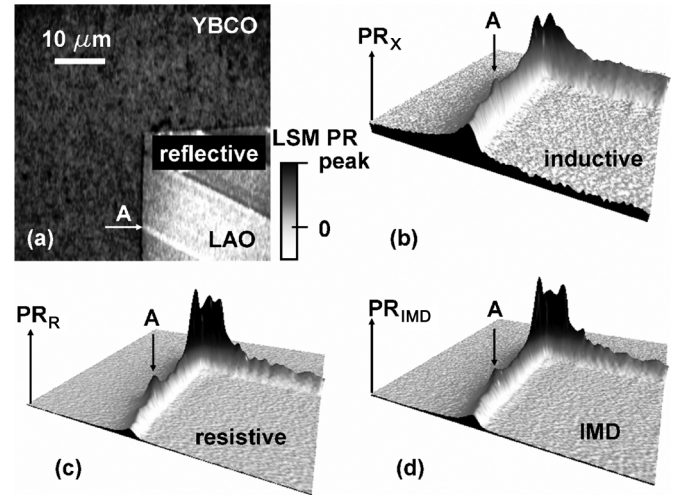
Fig. 3. 2-D LTLSM images of (a) reflectivity map showing the twinned structure of the substrate along with distribution of (b) inductive, (c) resistive, and (d) IMD components of LSM PR obtained in the same $50\ \mu m \times 50\ \mu m^2$ area around the inner corners of the resonator structure.

III. RESULTS AND DISCUSSION

In our previous papers [6], [7] examining microwave resonators of complex meander-line geometry we have demonstrated that the local sources of microwave NLs are non uniformly distributed across the film, and that IMD PR is dominantly localized in only small regions of the HTS film having the highest HF current densities, $J_{HF}(x, y)$. These regions coincide with the inner corners of the resonator structure and can radically affect the linearity of the device performance.

Fig. 3(a) shows the optical reflectance LSM image collected in a $50\ \mu m \times 50\ \mu m$ area of maximum $J_{HF}(x, y)$. The inductive $PR_X(x, y)$ image in this area is shown in Fig. 3(b). The distribution of $PR_X(x, y)$ clearly shows the current bunching at the micro-strip edges and reaches two extrema corresponding to $J_{PEAK} \sim (3 - 4) \times 10^9$ A/m^2 close to the inner corner at $T = 78$ K, and $P_{f1} = P_{f2} = -6$ dBm. In addition, a spatial modulation of the $PR_X(x, y)$ is noticeable along the edges away from the corner. This may be caused by spatial variation of the magnetic penetration depth in different twin-domain blocks (TDB) of the HTS film formed as a result of twinning in the LAO substrate that is evident from Fig. 3(a) [8]. As an example, arrow "A" in Fig. 3 indicates the position of the interface between two TDB. A very small increase of the $PR_X(x, y)$ can be seen at this location.

In contrast, the resistive (see Fig. 3(c)) component, $PR_R(x, y)$, demonstrates a sharper distribution of the LSM PR. It is also attached to the areas of local $J_{HF}(x, y)$ peaks at the inner corner and at the TDB interfaces. The origin of resistive response at that TDB interface (see point "A") may be connected with easier HF vortex entry in the HTS strip through suppression of the edge (Bean-Livingston) barrier there.

Fig. 3(d) shows the 2D variation of NL (or IMD) LSM PR acquired simultaneously. With the exception of some details, there is spatial correlation between both sources of $PR_{IMD}(x, y)$ and $PR_R(x, y)$ visible in the images suggesting a significant resistive origin of the sources of NL response. Therefore, we studied

the HF power P_{IN}-dependent spatial evolution of the $PR_R(x, y)$ to see how the NL sources originate.

It is important to keep in mind that the total LSM PR originates from two independent (resistive and inductive) contributions. The $PR_R(x, y)$ component is directly related to photo-induced modulation of the inverse Q-factor of the resonator due to an increase in local Ohmic dissipation. On the other hand, the $PR_X(x, y)$ component is associated with the change of kinetic inductance leading to the effects of HF resonant frequency tuning [5]. For high-quality resonant devices (with $Q > 1000$) the inductive component of LSM PR dominates, and so we did not see any visible power-dependent redistribution of LSM PR (x,y) at frequencies f_1 and f_2. Under such conditions, it is very labor-intensive to work with the set of LSM images obtained at $f_1(P_{IN})$ and $f_2(P_{IN})$ to construct the $PR_R(x, y, P_{HF})$ using the method described in [5].

Here we propose a new procedure of rapid, spatially-resolved approximate identification of the $PR_R(x, y)$ component using a simpler experimental setup employing the crystal detector instead of the spectrum analyser in Fig. 1. In this case only a single input tone is used. The procedure is based on the sharp increase of the ratio PR_R/PR_X at a frequency close to f_0. Fig. 4(a) shows the frequency dependence of PR_R and PR_X, calculated from Eqs. (8) and (9) in [4] describing these responses in terms of laser-beam-induced changes of resistive and inductive components of LSM PR, respectively. This model was revised slightly to include the contribution of insertion loss (IL) contrast to LSM PR, as shown in Fig. 4(a). We made the approximation that the IL contribution is mainly resistive in nature and can be added to the total resistive LSM PR. With this assumption, the ratio PR_R/PR_X is plotted in Fig. 4(b). It is seen that this ratio may exceed 10^4 at $f_C \sim f_0$ compared to a value of 10^{-3} off resonance. Such an appreciable difference means that the LSM image obtained at f_A reflects mainly inductive HF properties of the resonator while the LSM image obtained at f_C shows the distribution of resistively-induced PR.

As an example, Fig. 4(c) illustrates the distribution of LSM PR around an inside corner of the resonator at fixed frequency $f_A = 5.9675$ GHz at $T = 78$ K, and $P_{fA} = -24$ dBm. This distribution almost perfectly repeats the inductive PR that was extracted using the method of component partition [5]. Fig. 4(d) shows a spatial modification of the LSM PR(x,y) profiles for the case when both resistive and inductive components become comparable in their influence at $f_B = 5.9682$ GHz close to f_0. In contrast, Fig. 4(e) obtained under the same conditions at $f_C = 5.9685$ GHz manifests the appearance of resistive LSM PR whose amplitude is much higher than the inductive component at $P_{IN}(f_C) = -24$ dBm. We establish that for input powers $P_{IN}(f_C) > -12$ dBm it was impossible to observe a difference between the $PR_R(x, y)$ distributions measured by both two- and one-tone imaging procedures. Thus, the excitation of the resonator at a single frequency $f_C = 5.9685$ GHz was used to image the spatial penetration of the resistive LSM PR into the HTS film at different input HF power.

Fig. 5 shows that the first resistive areas in the HTS film form around the inside corner on a curved line for $P_{IN}(f_C) \leq 0$ dBm inside the strip edge. By comparison with the $PR_X(x, y)$ distribution (not shown) in this 25×25 μm^2 area it was de-
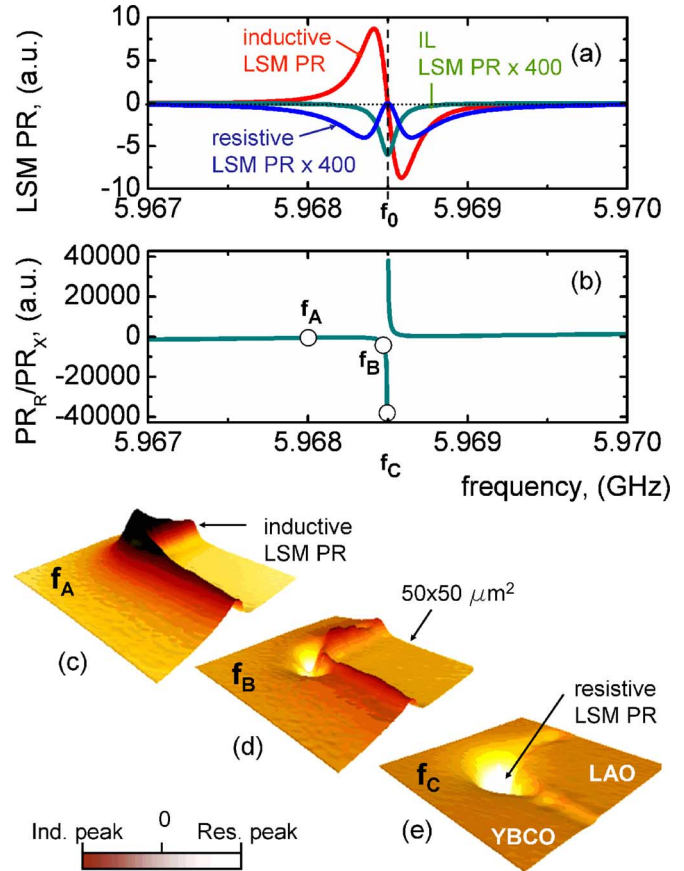

Fig. 4. Frequency dependence of (a) resistive, inductive and insertion loss (IL) components of LSM PR, (b) ratio of the sum of resistive and IL to inductive components, and 2D LSM images showing (c) image of mainly inductive LSM PR at f_A far from f_0, (d) image with comparable amplitudes of resistive and inductive LSM PR components at f_B closer to f_0 and (e) mainly resistive contribution at f_C almost equal to f_0.

termined that the position of the resistive line coincides with the regions of the HTS film carrying the highest $J_{HF}(x, y)$. With increasing $P_{IN}(f_C)$ from $+2$, $+4$ and then $+6$ dBm, the $PR_R(x, y)$ occupies increasingly more area of the HTS film surrounding the inner corner of the resonator structure. It is seen that the $PR_R(x, y)$ contrast has a very sharp front inside the HTS film and a smooth decay toward the patterned edges. The same resistive patterns were observed at all the corners of this resonator and in other HTS structures of meandering geometry imaged earlier. This is reminiscent of the development of an rf critical state in the film.

Such behavior is similar to that observed as a large disturbance of the flux pattern produced by increasing the applied magnetic field around macroscopic individual defects near the strip edge [9]. Here the role of the defect is played by the nearly zero-radius corners creating very large values of $J_{HF}(x, y)$ as a result of the sharp curvature of HF current flow. However, here we can not confirm the magnetic origin of the resistive domains due to the fact that the inductive $PR_X(x, y)$ does not change its shape at any P_{IN} applied up to $+12$ dBm. Also, we did not detect clear trajectories of magnetic penetration or the influence of TDBs on the formation of the resistive pattern. One possible explanation is current-induced resistive dissipation in zones of preferred HF vortex penetration and hysteresis [10]. A definitive
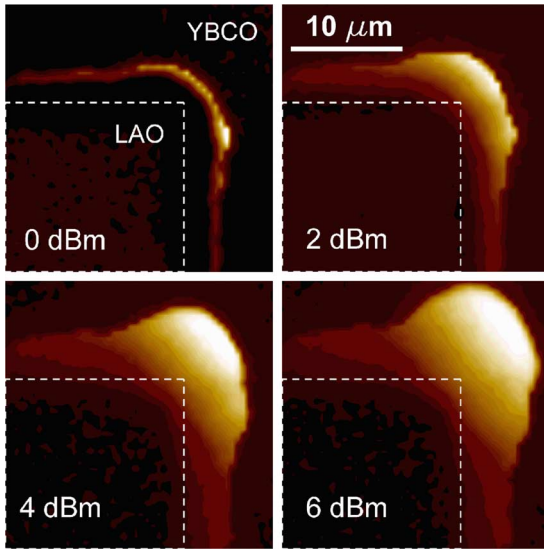
Fig. 5.   Images of resistive LSM PR penetrating into the inside corner of an HTS film at the different input HF powers indicated in the images. White dotted boxes show the YBCO/LAO patterned edge. Brighter regions correspond to larger amplitude of $PR_R(x,y)$.
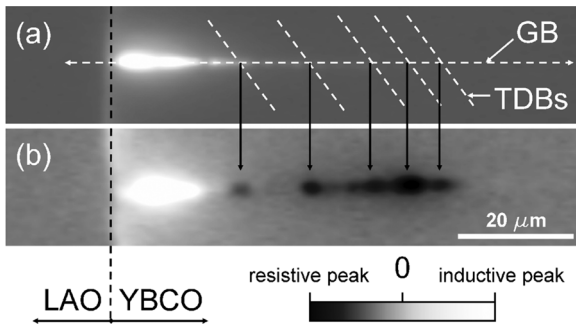

Fig. 6.   2D patterns of LSM PR obtained at 78 K, $+10$ dBm in a $125 \times 25\ \mu m^2$ area of the HTS resonator in the (a) absence and (b) presence of DC magnetic field. Bright (dark) spots correspond to inductive (resistive) response while grey regions are of zero PR signal. The edge of the strip is indicated by the black dashed line. Positions of the GB and TDBs coincide with the white dashed lines.

answer may be established by combining these results with measurements of the same resonator in other LSM dc/HF imaging modes [4]. The role of resistive nonlinearity at lower power [1], and in the absence of sharp corners, remains an open issue.

To show the difference between (i) HF current and (ii) magnetic-field-induced sources of resistive NL, we studied the spatial and power-dependent evolution of $J_{HF}(x,y)$ and resistive zones in the HTS resonator in the presence and absence of external static magnetic field. Fig. 6(a) shows a $125 \times 25\ \mu m^2$ map of LSM PR of the zero-field-cooled (to 78 K) resonator obtained at $f_1 = 5.968$ GHz in the area including a natural grain boundary (GB) marked by the horizontal white dashed line. This GB starts from the strip edge (black dashed line) and crosses the interfaces of TDBs (white dashed bevels) through the whole HTS structure. Only the inductive component (seen as a bright elongated spot along the GB) of LSM PR(x,y) was de-

tected in this environment in the range of applied HF power from -40 dBm to $+10$ dBm. The shape of this pattern was practically independent of P_{IN} and has the typical $J_{HF}(x,y)$ peak near the edge and characteristic spatial modulation along TDBs [8].

Fig. 6(b) shows the distribution of LSM PR modified at $P_{IN} = +10$ dBm by a c-oriented, DC magnetic field of strength 2–10 G from a permanent magnet. A radical transformation of the LSM PR(x,y) map is evident. The inductive pattern looks brighter due to the DC magnetic field suppressing the critical current in the GB. Dark resistive areas have been created by introduction of vortices at the intersection of the GB and TDBs shown by black arrows. The size of the resistive domains is equal to the size of the laser probe showing that the vortices are strongly pinned by the defects of the HTS structure. This feature clearly shows the difference between dc magnetically-derived resistivity, which is frequently used to explain NL properties of HTS films, and the HF current-induced losses like those presented in Fig. 5.

REFERENCES

[1] D. E. Oates, S.-H. Park, and G. Koren, "Observation of the nonlinear Meissner effect in YBCO thin films: Evidence for a d-wave order parameter in the bulk of the cuprate superconductors," *Phys. Rev. Lett.*, vol. 93, p. 197001, 2004.

[2] J. McDonald, J. R. Clem, and D. E. Oates, "Critical-state model for harmonic generation in a superconducting microwave resonator," *Phys. Rev. B.*, vol. 55, pp. 11823–11831, 1997.

[3] A. P. Zhuravel, S. M. Anlage, and A. V. Ustinov, "Microwave current imaging in passive HTS microwave components by low-temperature laser scanning microscopy (LTLSM)," *Journal of Superconductivity* [Online]. Available: http://www.dx.doi.org/10.1007/s10948-006-0123-5 (in press), (cond-mat/0311511)

[4] A. P. Zhuravel, A. G. Sivakov, O. G. Turutanov, A. N. Omelyanchouk, S. M. Anlage, A. Lukashenko, A. V. Ustinov, and D. Abraimov, "Laser scanning microscopy of HTS films and devices (review article)," *Low Temperature Physics*, vol. 32, pp. 592–607, June 2006.

[5] A. P. Zhuravel, S. M. Anlage, and A. V. Ustinov, "Measurement of local reactive and resistive photoresponse of a superconducting microwave device," *Appl. Phys. Lett.*, vol. 88, p. 212503, 2006.

[6] A. P. Zhuravel, A. V. Ustinov, D. Abraimov, and S. M. Anlage, "Imaging local sources of intermodulation in superconducting microwave devices," *IEEE Trans. Appl. Supercond.*, vol. 13, pp. 340–342, June 2003.

[7] A. P. Zhuravel, S. Remillard, S. M. Anlage, F. L. Barkov, and A. V. Ustinov, "Spatially resolved analyses of microwave and intermodulation current flow across HTS resonator using low temperature laser scanning microscopy," in *MSMW'04 Proceedings*, June 2004, vol. 1, pp. 421–423 [Online]. Available: http://www.dx.doi.org/10.1109/MSMW.2004.1345915

[8] A. P. Zhuravel, A. V. Ustinov, K. S. Harshavardhan, and S. M. Anlage, "Influence of $LaAlO_3$ surface topography on RF current distribution in superconducting microwave devices," *Appl. Phys. Lett.*, vol. 81, pp. 4979–4981, 2002.

[9] C. Jooss, J. Albrecht, H. Kuhn, S. Leonhardt, and H. Kronmuller, "Magneto-optical studies of current distributions in high-T_c superconductors," *Rep. Prog. Phys.*, vol. 65, pp. 651–788, 2002.

[10] J. McDonald, J. R. Clem, and D. E. Oates, "Critical-state model for intermodulation distortion in a superconducting microwave resonator," *J. Appl. Phys.*, vol. 83, pp. 5307–5312, May 15, 1998.